References and Notes

1. See list in R. M. Barker, thesis, University of California, Berkeley (1970).
2. H. C. Fritts, *Tree Rings and Climate* (Academic Press, New York, 1976).
3. C. Emiliani, J. H. Hudson, E. A. Shinn, R. Y. George, *Science* **202**, 627 (1978).
4. D. S. Jones, *Paleobiology* **6**, 331 (1980).
5. D. S. Jones *et al.*, *Mar. Biol.* **47**, 63 (1978).
6. D. S. Jones, thesis, Princeton University (1980).
7. J. F. Caddy and A. R. Billard, *Tech. Rep. Mar. Envir. Data Serv. Can.* **648** (1976), p. 1.
8. The von Bertalanffy growth curve is described by $y_t = y_\infty (1 - e^{-kt})$ where t is time in years, y is shell height, y_∞ is maximum shell height, k is a constant determined by curve fitting, and e is the base of the natural logarithms.
9. All specimens were captured alive so that each annual growth increment of the shell could be assigned to a specific calendar year. The shell height for each year of growth of each specimen was measured on shells sectioned radially (4148 measurements). The change in shell height for every year of growth (annual growth increment size) for each specimen was calculated as the difference between successive shell heights. An exponential decay curve was fitted to these data by a least-squares regression on the logarithmically transformed data. In all cases a correlation coefficient $r > .9$ was obtained. The yearly changes in shell height measured were converted to standardized indices (Fig. 2A) by dividing each by the expected growth. This division removes the ontogenetic growth trend and scales the variance so that it remains constant throughout the series, thus yielding standardized yearly indices that can be compared between individuals of any size (age).
10. J. G. Loesch and J. W. Ropes, *Proc. Natl. Shellfish. Assoc.* **67**, 29 (1977).
11. D. R. Franz, *Limnol. Oceanogr. Spec. Symp.* **2**, 404 (1976).
12. Small (young) clams are not represented in Fig. 2 because my samples came from commercial catches, and clammers must observe legal minimum size limits. Because of the favorable growing period around 1976 (Fig. 2A), a correspondingly good recruitment period is predicted for this time. This cannot be tested by the method described in this report until clams that settled in 1976 are large enough to be harvested. However, H. H. Haskin, R. R. Schneider, and M. Tarnowski [*Proc. Natl. Shellfish Assoc.* **69**, 195 (1979)], who studied recruitment in populations of inshore surf clams from New Jersey, describe 1976 as the first year of significant survival of juveniles after several very poor years.
13. W. S. Fairbridge, *Aust. J. Mar. Freshwater Res.* **4**, 1 (1953); J. Green, *J. Mar. Biol. Assoc. U.K.* **36**, 41 (1957); R. Seed, *Oecologia (Berlin)* **3**, 317 (1969).
14. W. R. Coe, *J. Exp. Zool.* **99**, 1 (1945); V. G. Loosanoff, *Biol. Bull. (Woods Hole, Mass.)* **114**, 57 (1958).
15. W. R. Coe, *J. Mar. Res.* **7**, 586 (1948); D. M. Pratt and D. A. Campbell, *Limnol. Oceanogr.* **1**, 2 (1956).
16. D. Leighton and R. A. Boolootian, *Ecology* **44**, 227 (1963).
17. K. M. Wilbur and G. Owen, in *Physiology of Mollusca*, K. M. Wilbur and C. M. Yonge, Eds. (Academic Press, New York, 1964), vol. 1, pp. 211-242.
18. Raw sea surface temperature data are ship injection temperatures collected and assembled into monthly means for the 1° area of latitude and longitude covering the central to southern New Jersey coast by the National Weather Records Center, Asheville, N.C. Because GI-1 forms in late summer to fall, the calendar years were divided into 12-month periods beginning in August and ending in July of the following year. Monthly mean sea surface temperatures were averaged over this interval for Fig. 2A.
19. Pearson product-moment correlation coefficient: $r = -.91$, $P < .01$. The zeroth-order serial correlation coefficient (no lag in years): $r = -.93$, $P < .01$. Higher order coefficients were not significant. Correlations between growth and maximum, minimum, and standard deviation of monthly sea surface temperatures were also not significant.
20. I. Thompson and D. Jones, *Geol. Soc. Am. Annu. Meet. Abstr. Program* **9**, 1199 (1977).

21. I thank J. Carter, G. Clark II, A. G. Fischer, H. Sachs, I. Thompson, and C. Jones. Supported by NOAA sea grants 04-6-158-44076 and 04-7-158-44042, NSF EAR 77-23571, and a Sigma Xi grant-in-aid of research.

16 January 1980; revised 9 June 1980

Relative Humidity: Important Modifier of Pollutant Uptake by Plants

Abstract. *Laboratory measurements of foliar uptake of sulfur dioxide and ozone by red kidney beans demonstrated a strong effect of relative humidity on internal pollutant dose. Foliar uptake was enhanced two- to threefold for sulfur dioxide and three- to fourfold for ozone by an increase in relative humidity from 35 to 75 percent. For the same exposure concentration, vegetation growing in humid areas (such as the eastern United States) may experience a significantly greater internal flux of pollutants than that in more arid regions.*

Plant susceptibility to air pollution stress is strongly influenced by environmental variables including air temperature, wind speed, light intensity, soil fertility, and soil and atmospheric moisture levels (*1-4*). The supply of moisture to vegetation both before and during exposure has been recognized for many years as one of the the most important of these variables (*5-11*). Conditions that minimize plant moisture stress, such as high soil moisture and high atmospheric humidity, generally increase plant susceptibility to foliar injury by air pollutants. Subtle pollutant effects on physiological processes, such as photosynthesis and transpiration, may also be enhanced by high humidity (*12*).

Although regional differences in average annual humidity have been implicated in the greater sensitivity of vegetation to air pollution in the humid eastern United States (*9, 13*), the physiological mode by which this environmental variable controls pollutant-plant interactions is not well understood. Mechanistically, vegetation may react to increased humidity by (i) enhanced uptake of pollutants, (ii) greater physiological sensitivity to the same level of pollutant uptake, or (iii) a combination of (i) and (ii).

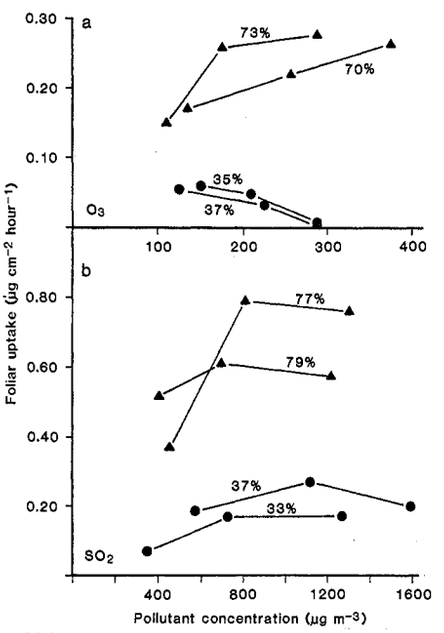

Fig. 1. Foliar uptake of O_3 (a) and SO_2 (b) as influenced by relative humidity and pollutant concentration. Results shown represent two exposures (ten plants each) at each humidity and pollutant combination.

Laboratory experiments were performed to determine the basis for humidity-induced variations in plant sensitivity to SO_2 and O_3. Eight groups of ten greenhouse-grown bush beans, *Phaseolus vulgaris* (Bush Blue Lake variety 274), were exposed in open gas-exchange chambers (*14*) to three concentrations of SO_2 (range, 350 to 1550 $\mu g\ m^{-3}$) or O_3 (range, 100 to 375 $\mu g\ m^{-3}$). Pollutant concentrations were maintained for 1 hour before measurement of uptake and progression to the next higher concentration. Relative humidity was held at 35 ± 2 or 75 ± 5 percent in two replicate chambers for each of the two pollutant series. Concurrent measures of both total pollutant flux and CO_2 assimilation (photosynthesis) were determined from mass balance calculations based on concentrations of gas entering and leaving the chambers. To determine physiological uptake, total flux calculations were corrected for adsorptive loss to both chamber walls and external leaf surfaces (*14*).

The effects of a 40 percent increase in humidity on uptake of both SO_2 and O_3 were pronounced at all gas concentrations (Fig. 1). Average SO_2 uptake was enhanced approximately 250 percent, and O_3 uptake was increased 400 percent. Maximum O_3 uptake (0.28 $\mu g\ cm^{-2}\ hour^{-1}$) occurred at a concentration of 150 $\mu g\ m^{-3}$ (0.079 ppm); the corresponding maximum for SO_2 (0.80 $\mu g\ cm^{-2}\ hour^{-1}$) occurred at 800 $\mu g\ m^{-3}$ (0.31 ppm). Uptake of both SO_2 and O_3 increased with the initial increase in exposure concentration in all treatments except O_3 at low relative humidity. With the latter treatment O_3 uptake decreased as the O_3 concentration increased. As pollutant concentrations increased further, uptake did not increase proportionally, but actually declined in all treatments except O_3 at high relative humidity.

Nonproportional uptake with increas-

0036-8075/81/0109-0167$00.50/0

Table 1. Effects of humidity and pollutant concentration on ratios of leaf conductance of O_3 and SO_2 to CO_2. Data are means ± 1 standard deviation of values determined from a linear least-squares fit to each of the replicate concentration series at each humidity. Humidity is the average value of replicate series and Ps represents percentage of prefumigation photosynthetic levels.

Pollutant concentration ($\mu g\ m^{-3}$)	Humidity (%)	Uptake		Humidity (%)	Uptake	
		Ratio to CO_2	Ps (%)		Ratio to CO_2	Ps (%)
		Ozone				
150		16.3 ± 2.1	111 ± 31		10.5 ± 3.9	92 ± 16
200	72	14.5 ± 2.2	111 ± 38	35	6.9 ± 3.0	89 ± 27
280		11.7 ± 2.4	111 ± 24		0.9 ± 1.6	84 ± 44
		Sulfur dioxide				
600		12.7 ± 3.0	93 ± 20		4.3 ± 0.7	103 ± 21
900	78	10.6 ± 1.1	86 ± 17	35	3.9 ± 0.3	94 ± 11
1200		8.5 ± 0.8	79 ± 14		3.5 ± 0.1	84 ± 1

ing concentration indicated that either stomatal resistance had increased due to stomatal closure, or resistance to movement through the mesophyll cells in the substomatal cavity had increased. Stomatal closure can be induced by exposure to SO_2 (*15*) or O_3 (*16, 17*) and has been hypothesized to be a protective mechanism for plants under pollutant stress (*17*). It is most frequently induced when plants are exposed at low humidity (*18*), but may be a much less significant factor than changes in mesophyll resistance (*12*) in limiting entry of CO_2 into photosynthesizing leaf cells exposed to SO_2. Mesophyll resistances to SO_2 and O_3 are generally considered to be quite low (*19*); however, little is known about how these resistances change under pollution stress.

To test the extent to which stomatal closure may have limited pollutant uptake, SO_2 and O_3 leaf conductances [uptake ($\mu g\ cm^{-2}\ hour^{-1}$)/concentration ($\mu g\ cm^{-3}$) = $cm\ hour^{-1}$] were compared with leaf conductances for CO_2 in photosynthesis (Table 1). Four main points may be made from the data shown in Table 1: (i) pathway conductances for O_3 and SO_2 were greater than those for CO_2; (ii) average conductance ratios of both SO_2 and O_3 were increased at high humidity, indicating that pollutant uptake was enhanced more than CO_2 uptake; (iii) pollutant/CO_2 conductance ratios decreased with increasing gas concentration, indicating preferential reduction in pollutant versus CO_2 uptake as a function of pollutant dose (a function of both instantaneous pollutant concentration and previous exposure in this experiment); and (iv) this reduction was much more apparent with O_3 than SO_2 and occurred over a concentration range (200 to 280 $\mu g\ m^{-3}$) within which photosynthesis was only slightly reduced.

Greater relative effects of humidity on conductance ratios than on photosynthesis indicate that changes in internal leaf resistance were primarily responsible for reduced O_3 uptake at higher O_3 concentrations. Calculations of leaf resistance changes based on the Ohm's law analogy [flux = (air-to-leaf concentration gradient)/(leaf resistance)] indicated that total leaf resistance [both stomatal and mesophyll (*20*)] to O_3 increased approximately 46 percent (2.7 to 4.0 sec cm^{-1}) at high humidity and 833 percent (10.8 to 101 sec cm^{-1}) at low humidity as the O_3 concentration was increased from 150 to 280 $\mu g\ m^{-3}$. Photosynthetic rate dropped very little over the same concentration range.

Our data indicate that altered rates of pollutant uptake by foliage may be the primary cause of humidity-induced variations in plant sensitivity to air pollutants. Furthermore, under our experimental conditions, the mechanism for these differences was altered internal leaf resistance to uptake, rather than stomatal regulation. These alterations may be a function of the influence of humidity on water flux through the leaf, as suggested by Barton *et al.* (*12*). Decreased uptake may also be a function of increased nonstomatal components of leaf resistance after periods of low soil moisture. Both increased resistance of plants to SO_2 (*11*) and decreased foliar uptake of sulfur (*8*) were reported in plants stressed by low soil moisture.

Thus, vegetation in regions of the country with dissimilar atmospheric and soil moisture regimes may receive very different internal pollutant doses at the same level of air pollution. Vegetation growing in arid areas may be protected from uptake of water-soluble pollutants by several physiological mechanisms. When soil moisture is low, leaf resistance to gaseous uptake is high. Stomatal closure may also be induced under these conditions when pollutants, particularly O_3, are present. Our data and those of Barton *et al.* (*12*) suggest that high rates of evapotranspiration, which would occur during periods when soil moisture is available and humidity is (typically) low, would protect plants from pollutant uptake. The eastern United States, where temperature, humidity, soil moisture, pollutant emissions, and the frequency of air stagnation events are high, has a greatly enhanced potential for air pollution damage to vegetation (*21*).

The influence of environmental variables on plant sensitivity to air pollutants suggests that air quality standards designed to protect vegetation might be tailored to consider variations in regional environmental conditions. The strong influence of relative humidity on foliar uptake of pollutant gases suggests that this variable could eventually provide a realistic basis for establishing such variances.

S. B. McLaughlin, G. E. Taylor
Environmental Sciences Division,
Oak Ridge National Laboratory,
Oak Ridge, Tennessee 37830

References and Notes

1. J. H. Bennett and A. C. Hill, in *Responses of Plants to Air Pollution*, J. B. Mudd and T. T. Kozlowski, Eds. (Academic Press, New York, 1975), pp. 273-306.
2. W. W. Heck, J. A. Dunning, I. J. Hindawi, *J. Air Pollut. Control Assoc.* **15**, 511 (1969).
3. H. E. Heggestad and W. W. Heck, in *Advances in Agronomy*, N. C. Brady, Ed. (Academic Press, New York, 1971), pp. 00-00.
4. A. C. Hill, *J. Air Pollut. Control Assoc.* **21**, 341 (1971).
5. J. A. Dunning and W. W. Heck, *Environ. Sci. Technol.* **7**, 824 (1973).
6. H. M. Hull and F. W. Went, *Proc. 2nd Natl. Air Pollut. Symp.* (1952), p. 122.
7. D. C. MacLean, R. E. Schneider, D. C. McCune, *Proc. 3rd Int. Clean Air Congr.* (1973), p. 143.
8. A. Markowski, S. Grzesiak, M. Schramel, *Bull. Acad. Pol. Sci. Ser. Sci. Terre* **22** (No. 12), 889 (1975).
9. H. W. Otto and R. H. Daines, *Science* **163**, 1209 (1969).
10. M. D. Thomas and R. H. Hendricks, in *Air Pollution Handbook*, P. L. Magill, F. R. Holden, C. Ackley, Eds. (McGraw-Hill, New York, 1956), sect. 9-1-9-44.
11. M. Schramel, *Bull. Acad. Pol. Sci. Ser. Sci. Terre* **13** (No. 1), 57 (1975).
12. J. R. Barton, S. B. McLaughlin, R. K. McConathy, *Environ. Pollut.* **21**, 255 (1980). After absorption in water on mesophyll cell walls, the inward movement of pollutant gases is influenced by both the water status of cell walls and cell membrane characteristics. At low atmospheric humidity, enhanced outward flow of transpired water through cell walls would provide a resistance to inward, liquid-phase diffusion.
13. H. E. Heggestad, F. R. Burleson, J. T. Middleton, E. F. Darley, *Int. J. Air Water Pollut.* **8**, 1 (1964).
14. The exposure chambers were 1.5-m^3 cylinders covered with Teflon with negative-pressure airflow at 0.15 $m^3\ min^{-1}$. Air within the chambers was continuously stirred by an impeller, providing uniform, gentle movement of all leaves within the canopy. Chamber air temperature was 30° ± 1°C and the level of photosynthetically active radiation (400 to 700 μm) was approximately 300 microeinsteins per square meter per second at plant height. Humidity was controlled by addition of steam. Vapor pressure deficits at relative humidities of 35 and 75 percent and an air and leaf temperatures of 30°C were approximately 1 and 2.7 kPa, respectively. Uptake of pollutants by plants and chamber walls was de-

termined in the dark at each humidity level. The values were used as estimates of surface-adsorbed pollutant flux in the light and were subtracted from total pollutant flux in the light to calculate uptake into plant leaves.
15. A. C. Hill and N. Littlefield, *Environ. Sci. Technol.* **1**, 52 (1969).
16. S. Rich and N. C. Turner, *J. Air Pollut. Control Assoc.* **22**, 718 (1972).
17. M. Mansfield and O. Majernik, *Environ. Pollut.* **3**, 1 (1970).
18. J. Bonte and P. Louguet, *Physiol. Veg.* **13**, 1 (1970).
19. A. C. Chamberlain, in *Air Pollutants and Their Effects on the Terrestrial Ecosystem*, S. V. Krupa and A. H. Legge, Eds. (Wiley-Interscience, New York, in press).
20. Leaf resistance is comprised of a gas-phase resistance and a series of liquid-phase (residual) resistances between initial absorption of the pollutant in the water on mesophyll walls and its initial biochemical reactions. These residual resistances are collectively referred to as mesophyll resistance. Changes in mesophyll resistance calculated by the Ohm's law formula may also be caused by internal factors that alter the leaf concentration of the gas in question and the air-leaf concentration gradient. Separation of resistance and gradient-induced changes in uptake is not generally attempted and not within the scope of this report.
21. D. S. Shriner *et al.*, *Oak Ridge Natl. Lab. Rep. ORNL/TM-5919* (1977).
22. Research sponsored by the U.S. Environmental Protection Agency under interagency agreement 40-740-78 and by the U.S. Department of Energy under contract W-7405-eng-26 with Union Carbide Corporation. Publication 1629, Environmental Sciences Division, Oak Ridge National Laboratory.

30 July 1980; revised 17 October 1980

Phosphorus Distribution in the Nucleosome

Abstract. *The spatial distribution of phosphorus within active fraction nucleosomes reveals that the path of the DNA is consistent with one and three-fourths turns of DNA supercoiled around the outside of the protein core. This phosphorus distribution, obtained with an imaging electron spectrometer in a conventional transmission electron microscope, simultaneously establishes new limits of sensitivity for elemental microanalysis.*

We have adapted a high-resolution electron microscope with an imaging electron energy spectrometer capable of resolving structural information of biological specimens to at least the 0.5-nm level while supplying chemical information with the same spatial resolution (*1*). The electron spectrometer allows an electron micrograph to be formed by using electrons that have lost a discrete amount of energy as a result of interactions with a particular chemical element or chromophore in the specimen. We have used this instrument to study the DNA distribution in the subunits of eukaryotic chromatin known as nucleosomes. We are able to locate the path of the DNA within the nucleosome and between nucleosomes by electron spectroscopic imaging that makes use of an energy loss due to phosphorus. Since phosphorus is primarily found in the DNA and not in the proteins constituting the particle, an image of the phosphorus distribution is predominantly an image of the DNA within the nucleosome.

The chromatin was prepared from calf thymus and enriched for active fraction chromatin by deoxyribonuclease II digestion and Mg^{2+} solubility (*2*). The buffer containing the chromatin was adjusted to 0.35*M* NaCl to remove the high-mobility group (HMG) proteins. The oligomers of nucleosomes were then separated from the free proteins by chromatography (Sepharose 4B, Pharmacia). Microscope grids of unstained chromatin were prepared as described (*3*), and micrographs were obtained with axial illumination at the desired energy loss, a dose of about 1.4 coulombs per square centimeter being used to form each image.

Electrons interacting with phosphorus have characteristic energy losses corresponding to K-shell and L-shell excitations of the phosphorus atoms. We have used the relatively strong $L_{2,3}$ excitations at 132 eV. In the electron energy loss spectrum, this specific phosphorus L-edge absorption is superimposed on a rapidly declining general background of localized and delocalized electron-scattering events. The effect of this background signal was eliminated by forming two consecutive images of the same region, one on the phosphorus L edge and one with an energy just below the edge. The latter image, normalized in intensity, must then be subtracted from the former to obtain a net phosphorus signal.

Figure 1 shows two images of the same strand of nucleosomes. One image (Fig. 1a) was formed at an energy loss of 155 eV, just above the L edge at 132 eV, referred to as the phosphorus spectroscopic image, and the other (reference) image (Fig. 1b) at an energy loss of 105 eV. The two images are nearly identical. However, close examination shows fine structural detail in one image that is not always duplicated in the other. The two images were digitized with a microdensitometer (Perkin-Elmer model 1010A) over regions containing the nucleosomes to give matrices of 4096 picture elements (64 × 64), each corresponding to 0.7 by 0.7 nm^2. Although the potential resolution of electron spectroscopic images is at least 0.7 nm (*1*), digitization with this pixel size limits the effective resolution of the images to 1.4 nm at worst. However, this is still sufficient for a DNA strand that is approximately 2 nm in thickness to be visualized. Before the subtraction was performed, one image was normalized to the other over the background to compensate for slightly different exposures. In addition, corresponding pairs of images were translationally cross-correlated in the computer to obtain the best overlap. Rotational cross-correlation was not necessary since consecutive images were sufficiently parallel.

We have studied 30 nucleosomes from one chromatin strand in detail, the first 13 of which are shown in Fig. 1 and the last 7 in Fig. 2a. In Fig. 2b, the computer-processed net phosphorus images have been superposed over the corresponding nucleosomes in the original phosphorus spectroscopic image. Al-

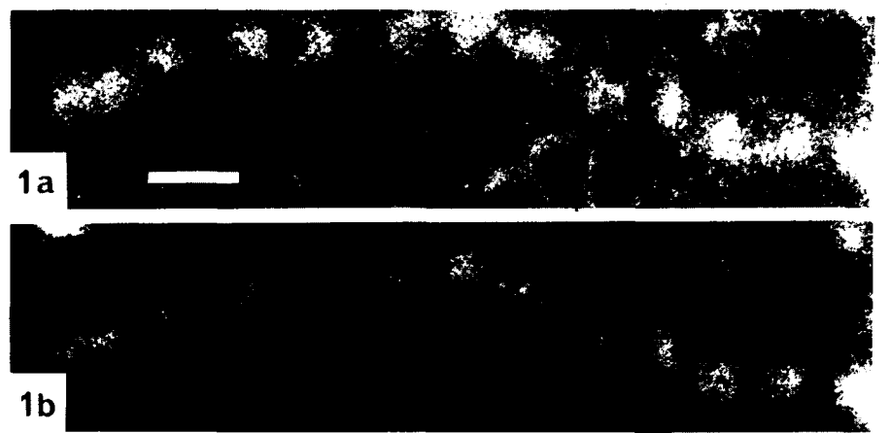

Fig. 1. (a) Phosphorus spectroscopic image of a strand of nucleosomes taken at an energy loss of 155 eV, just above the $L_{2,3}$ absorption edge of phosphorus. (b) Reference image of the same region shown in (a), taken at an energy loss of 105 eV. Scale bar, 30 nm.

0036-8075/81/0109-0169$00.50/0